IJRAR.ORG E-ISSN: 2348-1269, P-ISSN: 2349-5138

INTERNATIONAL JOURNAL OF RESEARCH AND ANALYTICAL REVIEWS (IJRAR) | IJRAR.ORG

An International Open Access, Peer-reviewed, Refereed Journal

Behaviour of Casson fluid on three-dimensional Nanofluid flow past a porous stretching sheet: Magnetic field, Nanofluid flow and Multiple slip effects

Ch. Janaiah [1], and B. Saidi Reddy

1 Department of Mathematics, Government Degree College, Alair, Yadadri Bhuvanagiri Dist, Telangana State, Pin 508101, India,

[*] Department of Mathematics, K.R.R.Govt. Arts & Science College (A), Kodad, Suryapet (Dt), Telangana State, 508206, India,

DOI: https://doi.org/10.56975/ijrar.v13i1.332387

Abstract:

This work used computational techniques to examine a three-dimensional, viscous, incompressible, electrically conducting, laminar fluid flow originating from a flexible sheet inside a nanofluid exposed to a magnetic field and characterized by perforations. The nanofluid model utilizes the Buongiorno model, including thermophoresis and Brownian motion. Similarity variables are used to convert non-linear partial differential equations into third-order partial differential equations. MATLAB's "bvp4c" is used to solve the flow variables, which include graphs of primary and secondary velocities, temperatures, and concentrations. This is how converted third-order differential equations are made. A picture shows how flow field variables and certain developing parts are related. Tables demonstrate the study's results, which include mass transfer values, velocity rates, and non-dimensional heat transfer. The topic of this research has immediate applications in the cooling of transformers, generators, and electrical equipment.

Keywords: Casson fluid; Nanofluid; MHD; Multiple slips; Porous medium; Three-dimensional;

Nomenclature:

List of Symbols:

u, v, w **:** Velocity components in x, y and z axes respectively (m/s)

x, y, z **:** Cartesian coordinates measured along the stretching sheet (m)

f **:** Dimensionless stream function along x - direction $(kg / m.\ s)$

f' **:** Fluid velocity along x - direction (m/s)

g **:** Dimensionless stream function along y - direction $(kg / m.\ s)$

g' : Fluid velocity along y - direction (m/s)

Pr: Prandtl number

T: Fluid temperature (K)

T_w : Temperature at the surface (K)

B_o : Uniform magnetic field ($Tesla$)

M : Magnetic field parameter

T_∞ : Temperature of the fluid far away from the stretching sheet (K)

Cf : Skin-friction coefficient along x-direction (s^{-1})

$u_w(x)$: Stretching velocity of the fluid along x-direction (m/s)

$v_w(y)$: Stretching velocity of the fluid along y - direction(m/s)

Nu : Rate of heat transfer coefficient (or) Nusselt number

Sh : Rate of mass transfer coefficient (or) Sherwood number

C_p : Specific heat capacity of nano particles ($J / kg / K$)

a : Constant

Re_x : Reynolds number

C : Fluid nanoparticle volume concentration (mol/m^3)

C_∞ : Dimensional ambient volume fraction (mol/m^3)

Nb : Brownian motion parameter

Nt : Thermophoresis parameter

A: Coefficient related to stretching sheet

Le : Lewis number parameter

D_B : Coefficient of Brownian diffusion (m^2 / s)

C_w : Dimensional nanoparticle volume concentration at the stretching surface (mol/m^3)

D_T : Coefficient of Thermophoresis diffusion (m^2 / s)

n: Velocity power index parameter

k^*: Dimensional permeability parameter

K: Non-dimensional permeability parameter

L_1 : Velocity slip coefficient

L_2 : Thermal slip coefficient

Greek symbols:

η : Dimensionless similarity variable (m)

θ : Dimensionless temperature (K)

ν : Kinematic viscosity (m^2 / s)

σ : Electrical Conductivity

μ : Dynamic viscosity of the fluid

κ : Thermal conductivity of the fluid

ρ : Density of the fluid (kg / m^3)

τ : Effective heat capacitance

ϕ : Nanoparticle volume concentration at the stretching surface (mol/m^3)

δ_1 : Velocity slip parameter

δ_2 : Thermal slip parameter

τ : Cauchy Stress tensor

μ_B : Dynamic viscosity of the Casson fluid

μ : Dynamic viscosity of the fluid

α^* : Shear rate

τ_o : Stress tensor

τ_B : Shear stress

β : Casson fluid parameter

Superscript:

$'$: Differentiation w.r.t z

Subscripts:

f : Fluid

w : Condition on the sheet

∞ : Ambient Conditions

1. Introduction:

One distinctive boundary condition that is introduced by slip at fluid-solid interfaces is the overall flow characteristics, which are greatly affected. In contrast to the usual no-slip scenario at the solid-fluid interface, there are several kinds of slip effects in fluid dynamics, such as velocity slip, temperature slip, and concentration slip. Complicated analysis of many slip effects necessitates in-depth knowledge of how these effects interact with one another in fluid dynamics. Both natural and industrial processes are impacted by the thermal slip condition, which has a considerable impact on boundary layer flow. This encompasses not only the extrusion of metals and plastics, but also the chilling and drying processes involved in making paper and textiles. Heat exchangers, oil recovery, chamber chemical reactions, rectangular duct catalytic reactors, and surface chemical vapour deposition are some of the engineering applications impacted by these factors. Bioconvection, blood flow in tumours, bio-heat transfer in tissues during genesis, and diffusion in brain tissues are just a few examples of the many biological settings where flow models in porous media are used. Stanford, Mabood et al. [1] looked into what happens to magnetohydrodynamic uneven flow, heat, and mass transfer on a stretchable transparent sheet that is exposed to radiation when it slips over and over again. Using magnetic nanoparticles, Eleni et al. [2] looked into how many slips, Soret, and Dufour affect the flow of fluid along a vertically stretched sheet. In their study [3], Shahid Ali et al. looked into the magnetohydrodynamic axisymmetric buoyant nanofluid flow across a stretched sheet, looking at the effects of radiation and chemical reactions. The study looked at the different effects of a number of slips. Using the finite element method, Khan et al. [4] looked into what happens to magnetohydrodynamic turbulent viscous flow across a transparent stretched sheet with radiation when it slips over and over again. Soltani, Yilmazer, et al. [5] We looked at the flow of a concentrated solution and measured the slip velocity and slip layer thickness. A study by Sekhar et al. [6] looked into how radiation and Joule heating affected the magnetohydrodynamic boundary layer flow over a stretched sheet in a porous material. Atunmbi and Adeniyan et al. [7] looked at how heat and mass move through a stretched sheet when a magnetohydrodynamic micropolar fluid flows through it. They took thermal slip and velocity conditions into account. A study by Raju et al. [8] looked at how multiple slip and cross diffusion affect magnetohydrodynamics. The Carreau-Casson fluid is spread over a slanderous sheet that has a heat source or washbasin that is not even. Number eight. In their study [9], Hussain et al. looked at how nanofluids slip flow and move heat across a porous plate inside a porous medium, taking into account how viscosity and thermal conductivity change with temperature. There are nine. It was studied by Ganesh Kumar et al. [10] how the magnetic flow of Carreau nanofluid changes over time, looking at slip effects and nonlinear thermal radiation. In their study [11], Alsenafi and Ferdows looked at how thermal slip and chemical processes affected a free convective nanofluid that came from a flat plate that was inserted in a porous medium. Sajid et al. [12] used the modified Fourier theory—Reiner-Philipp off model to study how Maxwell velocity slip and Smoluchowski temperature slip affect carbon nanotubes. In their study [13], Aziz and Jamshed looked into the unstable magnetohydrodynamic slip flow of a non-Newtonian power-law nanofluid across a moving surface, taking into account how thermal conductivity changes with temperature. The effects of concentration loss, temperature, and speed on magneto-hydrodynamic nanofluid flow were studied by Awais et al. [14]. Researchers Mishra and Kumar [15] looked into how thermal slip and speed affect the flow of a magnetohydrodynamic nanofluid across a stretched cylinder. They looked at things like Joule heating and viscous dissipation. The collocation method was used by Usman et al. [16] to study how temperature and speed differences affected the flow of Casson nanofluid across an angled, transparent, stretched cylinder. A study by Abbas et al. [17] looked into how thermal sliding and speed affect the flow of a micropolar nano fluid boundary layer over a stretched Riga sheet that is not straight up and down. An experiment by Swain et al. [18] looked into the thermal slip effect and how a magnetohydrodynamic convective nanofluid flows across a vertical plate that is immersed in a porous medium. The optimal homotopy asymptotic method was used by Adem and Kishan [19] to look at how slip affects the flow and heat transfer of a nanofluid across a nonlinearly stretched sheet. A study by Salleh et al. [20] used Buongiorno's model to look into how slip-on mixed convection flow affects nanofluids with a small needle. Researchers Uddin et al. [21] looked at how a radiative convective nanofluid moved across a sheet that was growing and shrinking, taking into account the slip effect. To study the magnetohydrodynamic boundary layer slip flow of a chemically reacting and emitting nanofluid across a stretched sheet using Newtonian heating, Das et al. [22] did research. The work of Isa et al. [23] looked into how slip conditions affect the magnetohydrodynamics of the fluid coming from a sheet that is being stretched rapidly. Ramzan et al. [24] looked into how heat diffusion and slide affect the flow of fluid across a sloped plate.

This research builds on the work that has already been done and wants to find out how Brownian motion and thermophoresis affect the flow of a three-dimensional, steady, viscous, non-Newtonian Casson fluid along a deformable sheet that is embedded in a porous medium. The fluid can't be compressed and conducts electricity. The nanofluid model created by Buongiorno et al. [25], which includes many slip effects, will be used to do this. This work adds to Khan et al.'s [26] work by looking at the effects of magnetic field, Casson fluid, porous medium, Lewis number, velocity, and thermal slip. The highly nonlinear system of ordinary differential equations that is left is solved quantitatively using the "bvp4c" method in MATLAB. This paper carefully looks at how regulatory factors affect skin friction, heat transfer rate, and mass transfer at the surface, as well as the main, secondary, temperature, and concentration profiles. It does this using both math and graphs.

2. Basic Fluid Flow Governing Equations:

Specifically, this section looks at the speed and thermal slip effects on a three-dimensional, viscous, electrically conducting, non-Newtonian Casson fluid flow towards a deformable sheet when thermophoresis and Brownian motion effects are present. Numerical solutions were used to study these effects. Figure 1 displays the shape of the flowing flow. The following claims are made based on the results of this investigation:

$u \to 0,\ v \to 0,\ T \to T_\infty,\ C \to C_\infty$ z Casson + Nanofluidparticles

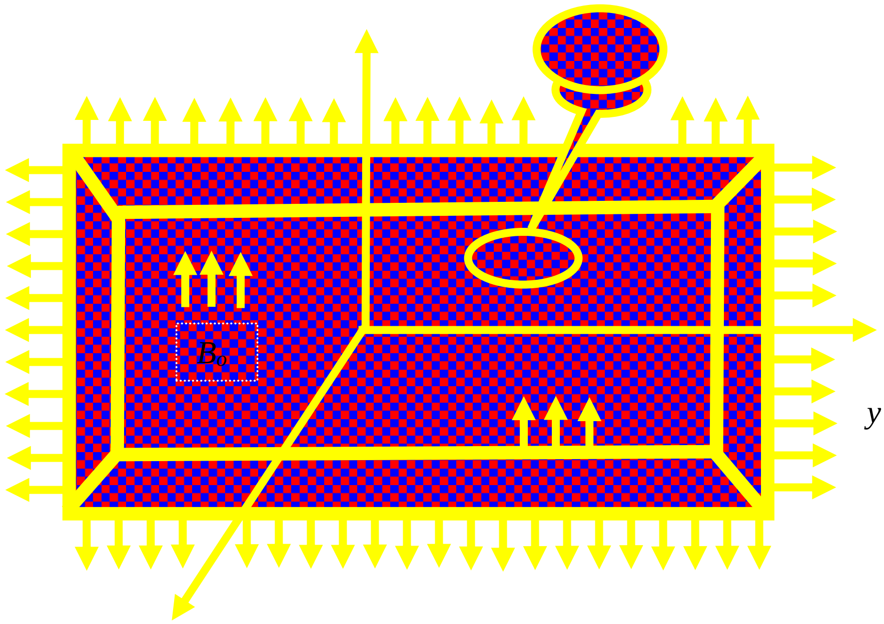

$$u = U_w = ax + L_1\left(\frac{\partial u}{\partial z}\right),\ v = V_w = by,\ w = 0,\ T = T_w + L_2\left(\frac{\partial T}{\partial z}\right),\ C = C_w$$

Fig. 1.: Coordinate system of Casson Nanofluid flow along a deformable sheet

a) When looking at the flexible sheet, the varying width is shown as $z = A\left(x + y + z\right)^{\frac{1-n}{2}}$.

b) Also, the sheet's stretched speed is $u_w = a\left(x + y + z\right)^{\frac{1-n}{2}}$, which works for $n \neq 1$ since n - 1 makes the flat flexible sheet less important.

c) This work assumes that the magnetic Reynolds number is very low.

d) In order to control the flow rate, the authors of this study opted to employ a B_o magnetic field.

e) The velocity slip is included into the momentum boundary condition.

f) There is now a temperature slip condition added to the energy equation border condition.

g) People who use the energy calculation don't take into account the effects of Dufour, sluggish loss, joule burning, and thermal radiation.

h) In species concentration equation, the effects of Soret and chemical reaction are neglected.

i) A non-Newtonian fluid's rheology equation looks like this:

$$\tau = \tau_o + \mu\alpha^* \tag{1}$$

Equation (1) can be expanded for Casson fluid as,

$$\tau_{ij} = \left\{ 2\left(\mu_B + \frac{p_y}{\sqrt{2\pi}}\right)e_{ij},\ \pi > \pi_c \ \&\ 2\left(\mu_B + \frac{p_y}{\sqrt{2\pi_c}}\right)e_{ij},\ \pi < \pi_c \right. \tag{2}$$

Where $\pi = e_{ij}e_{ji}$ with e_{ij} is the $(i,\ j)^{th}$ component of the fluid deformation rate and $p_y = \dfrac{\mu_B\sqrt{2\pi}}{\beta}$ is the yield stress of the Casson fluid.

According to the ideas we've talked about so far, these models should be used to control flow:

Equation for Continuity:

$$\frac{\partial u}{\partial x}+\frac{\partial v}{\partial y}+\frac{\partial w}{\partial z}=0 \tag{3}$$

Equations for Momentum:

$$u\left(\frac{\partial u}{\partial x}\right)+v\left(\frac{\partial u}{\partial y}\right)+w\left(\frac{\partial w}{\partial z}\right)=\nu\left(1+\frac{1}{\beta}\right)\left(\frac{\partial^2 u}{\partial z^2}\right)-\left(\frac{\sigma B_o^2}{\rho}\right)u-\left(\frac{\nu}{k^*}\right)u \tag{4}$$

$$u\left(\frac{\partial u}{\partial x}\right)+v\left(\frac{\partial u}{\partial y}\right)+w\left(\frac{\partial w}{\partial z}\right)=\nu\left(1+\frac{1}{\beta}\right)\left(\frac{\partial^2 v}{\partial z^2}\right)-\left(\frac{\sigma B_o^2}{\rho}\right)v-\left(\frac{\nu}{k^*}\right)v \tag{5}$$

The equation for heat energy is:

$$u\left(\frac{\partial T}{\partial x}\right)+v\left(\frac{\partial T}{\partial y}\right)+w\left(\frac{\partial T}{\partial z}\right)=\frac{\kappa}{\rho C_p}\left(\frac{\partial^2 T}{\partial z^2}\right)+\tau\left[D_B\frac{\partial T}{\partial z}\frac{\partial C}{\partial z}+\frac{D_T}{T_\infty}\left(\frac{\partial T}{\partial z}\right)^2\right] \tag{6}$$

The equation for species concentration is:

$$u\left(\frac{\partial C}{\partial x}\right)+v\left(\frac{\partial C}{\partial y}\right)+w\left(\frac{\partial C}{\partial z}\right)=D_B\left(\frac{\partial^2 C}{\partial z^2}\right)+\frac{D_T}{T_\infty}\left(\frac{\partial^2 T}{\partial z^2}\right) \tag{7}$$

The conditions at the flow's edges are

$$\left.\begin{array}{l} u=u_w(x)+L_1\left(\dfrac{\partial u}{\partial z}\right),\ \ v=v_w(x),\ \ T=T_w+L_2\left(\dfrac{\partial T}{\partial z}\right),\ \ C=C_w(x)\ \ at\ \ z=0 \\ u\to 0,\ \ v\to 0,\ \ T\to T_\infty,\ C\to C_\infty\ \ as\ \ z\to\infty \end{array}\right\} \tag{8}$$

Where $$\left.B(x)=B_o(x+y+z)^{\frac{1-n}{2}},\right\} \tag{9}$$

$$\left.\begin{array}{l} u_w=a(x+y+z)^{\frac{1-n}{2}},\ v_w=a(x+y+z)^n,\ \tau=\dfrac{(\rho C_p)_s}{(\rho C_p)_f}, \\ T_w=T_\infty+T_o(x+y+z)^{\frac{1-n}{2}},\ C_w=C_\infty+C_o(x+y+z)^{\frac{1-n}{2}}, \end{array}\right\}\ \ for\ \ n\neq 1 \tag{10}$$

The solutions you're looking for should become apparent after you apply the following similarity transformations to the governing equations, transforming them into ordinary differential equations.

$$\left.\begin{array}{l} u=a(x+y+z)^n f'(\eta),\ \theta=\dfrac{T-T_\infty}{T_w(x)-T_\infty},\ \phi=\dfrac{C-C_\infty}{C_w(x)-C_\infty},\ v=a(x+y+z)^n g'(\eta), \\ \eta=z\left(\sqrt{\dfrac{(n+1)a}{2\nu}}\right)(x+y+z)^{\frac{1-n}{2}}, \\ w=-\sqrt{\dfrac{2a\nu}{n+1}}(x+y+z)^{\frac{1-n}{2}}\left\{\left(\dfrac{n+1}{2}\right)\left[f(\eta)+g(\eta)\right]+\eta\left(\dfrac{n-1}{2}\right)\left[f'(\eta)+g'(\eta)\right]\right\} \end{array}\right\} \tag{11}$$

Equations (4), (5), (6), and (7) all make use of the following version of the continuity equation, which is supported by Equation (11).

$$\left(1+\frac{1}{\beta}\right)\left(\frac{n+1}{2}\right) f''' - nf'^2 - nf'g' + \left(\frac{n+1}{2}\right) ff'' + \left(\frac{n+1}{2}\right) gf'' - Mf' - Kf' = 0 \tag{12}$$

$$\left(1+\frac{1}{\beta}\right)\left(\frac{n+1}{2}\right) g''' - ng'^2 - nf'g' + \left(\frac{n+1}{2}\right) fg'' + \left(\frac{n+1}{2}\right) gg'' - Mg' - Kg' = 0 \tag{13}$$

$$\theta'' + Nb\theta'\phi' + Nt\theta'^2 - \left(\frac{1-n}{1+n}\right)\Pr f'\theta - \left(\frac{1-n}{1+n}\right)\Pr g'\theta + \left(\frac{1-n}{1+n}\right)\Pr f\theta' + \left(\frac{1-n}{1+n}\right)\Pr g\theta' = 0 \tag{14}$$

$$Nb\phi'' + Nt\theta'' + LeNb\left(\frac{1-n}{1+n}\right) f'\phi - NbLe\left(\frac{1-n}{1+n}\right) g'\phi + NbLe\left(\frac{1-n}{1+n}\right) f\phi' + NbLe\left(\frac{1-n}{1+n}\right) g\phi' = 0 \tag{15}$$

The following limits on the system's capabilities are enforced by this (6):

$$\left.\begin{array}{l} f(0)=0,\ g(0)=0,\ f'(0)=1+\delta_1 f''(0),\ g'(0)=1,\ \theta(0)=1+\delta_2\theta'(0),\ \phi(0)=1, \\ f'(\infty)=0,\ g'(\infty)=0,\ \theta(\infty)=0,\ \phi(\infty)=0, \end{array}\right\} \tag{16}$$

Several of the constituent parts of the topic under discussion are referred to as

$$\left.\begin{array}{l} M=\dfrac{\sigma B_o^2}{\rho a},\ \Pr=\dfrac{\mu C_p}{\kappa},\ Le=\dfrac{\nu}{D_B},\ Nb=\dfrac{\tau D_B\left(C_w-C_\infty\right)}{\left(\mu C_p\right)_f},\ \delta_2=\sqrt{\dfrac{ac}{\nu}} \\ Nt=\dfrac{\tau D_T\left(T_w-T_\infty\right)}{T_\infty\left(\mu C_p\right)_f},\ \delta_1=L_1\sqrt{\left(\dfrac{a}{\nu}\right)},\ K=\dfrac{\nu}{k^*} \end{array}\right\} \tag{17}$$

Using the information that has been provided, you may now determine the Sherwood number, the skin-friction coefficient, and the local Nusselt number.

$$\left.\begin{array}{l} Cf_x=2\sqrt{\dfrac{n+1}{2}}.\left(1+\dfrac{1}{\beta}\right)\dfrac{1}{\sqrt{\mathrm{Re}_x}}.\ f''(0),\ Cf_y=2\sqrt{\dfrac{n+1}{2}}.\left(1+\dfrac{1}{\beta}\right)\dfrac{1}{\sqrt{\mathrm{Re}_y}}.\ g''(0), \\ Nu=-\sqrt{\dfrac{n+1}{2}}.\sqrt{\mathrm{Re}_x}.\ \theta'(0),\ Sh=-\sqrt{\dfrac{n+1}{2}}.\sqrt{\mathrm{Re}_x}.\ \phi'(0) \end{array}\right\} \tag{18}$$

Where $\mathrm{Re}_x=\dfrac{u_x(x)(x+y+z)}{\nu}$ & $\mathrm{Re}_y=\dfrac{v_x(x)(x+y+z)}{\nu}$ are local Reynolds numbers.

3. Numerical Solutions by MATLAB ‘bvp4c’ technique:

Equations (12)–(15) illustrate the system of higher order non-linear ODEs, while Equation (16) shows the boundary conditions for rheology. The authors numerically solve these problems using the bvp4c approach, which is built on top of MATLAB. The Lobatto IIIA R-K approach is used to get accurate numerical answers of the fourth order. Three steps are involved. In order to include the bvp4c approach into our physical model, the following procedures were followed. Why is it important for streams to adhere to Newton's laws. The formula for non-Newtonian fluid rheology is

Step-1: Equations (12) and (15) are used to incorporate the additional elements into the system of higher order nonlinear ordinary differential equations.

$$\left.\begin{aligned} &y(1)=f,\ y(2)=f',\ y(3)=f'',\ y(4)=g,\ y(5)=g',\\ &y(6)=g'',\ y(7)=\theta,\ y(8)=\theta',\ y(9)=\phi,\ y(10)=\phi' \end{aligned}\right\} \tag{19}$$

Step-2: Utilising the additional variables in Equation (19), reduce the set of more complex non-linear ODEs in Eqn's (9)–(12) to a set of first-order, simpler ODEs.

$$f'''=\frac{n\left(y(2)\right)^2+ny(1)y(5)-\left(\frac{n+1}{2}\right)y(1)y(3)-\left(\frac{n+1}{2}\right)y(4)y(3)+My(2)+Ky(2)}{\left(1+\frac{1}{\beta}\right)\left(\frac{n+1}{2}\right)} \tag{20}$$

$$g'''=\frac{n\left(y(5)\right)^2+ny(2)y(5)-\left(\frac{n+1}{2}\right)y(1)y(6)-\left(\frac{n+1}{2}\right)y(4)y(6)+My(5)+Ky(5)}{\left(1+\frac{1}{\beta}\right)\left(\frac{n+1}{2}\right)} \tag{21}$$

$$\begin{aligned}\theta''=&-Nby(8)y(10)-Nt\left(y(8)\right)^2+\left(\frac{1-n}{1+n}\right)\Pr y(2)y(7)+\left(\frac{1-n}{1+n}\right)\Pr y(5)y(7)\\ &-\left(\frac{1-n}{1+n}\right)\Pr y(1)y(8)-\left(\frac{1-n}{1+n}\right)\Pr y(4)y(8)\end{aligned} \tag{22}$$

$$\phi''=\frac{\begin{aligned}&-Nt\left\{\begin{aligned}&-Nby(8)y(10)-Nt\left(y(8)\right)^2+\left(\frac{1-n}{1+n}\right)\Pr y(2)y(7)+\left(\frac{1-n}{1+n}\right)\Pr y(5)y(7)\\ &-\left(\frac{1-n}{1+n}\right)\Pr y(1)y(8)-\left(\frac{1-n}{1+n}\right)\Pr y(4)y(8)\end{aligned}\right\}\\ &-LeNb\left(\frac{1-n}{1+n}\right)y(2)y(9)+NbLe\left(\frac{1-n}{1+n}\right)y(5)y(9)\\ &-NbLe\left(\frac{1-n}{1+n}\right)y(1)y(10)-NbLe\left(\frac{1-n}{1+n}\right)y(4)y(10)\end{aligned}}{Nb} \tag{23}$$

Step-3: Using the new variables in Equation 19, write the border conditions in Equation 13.

$$\left.\begin{aligned}&\left[y(1)\right]_p=0,\ \left[y(4)\right]_p=0,\ \left[y(2)\right]_p=1+\delta_1\left[y(3)\right]_p,\ \left[y(7)\right]_p=1+\delta_2\left[y(8)\right]_p,\\ &\left[y(5)\right]_p=1,\ \left[y(9)\right]_p=1,\ \left[y(2)\right]_q=0,\ \left[y(5)\right]_q=0,\ \left[y(7)\right]_q=0,\ \left[y(9)\right]_q=0\end{aligned}\right\} \tag{24}$$

The positions on the sheet for $\eta = 0$ and the distances from the sheet for a certain value of η are indicated by the subscript's 'p' and 'q,' respectively. This site is under examination with a value of $\eta = 6$.

Step-4: The boundary conditions of equation (24) and the first-order nonlinear ordinary differential equations (ODEs) of equations (20)–(23) should be expressed using the bvp4c method.

Step-5: If you run the bvp4c method with various initial values, you may get the boundary conditions for the first and second solutions of the first-order nonlinear ODEs (equations (20)– (23)). Starting estimations are valid if computed velocity and temperature curves fit Eq. 16. The procedure is recommenced using alternate estimations in the event that they do not. The average number of attempts to generate a set of initial guesses is very high. Here is the bvp4c solution using Equation (24).

4. Program Code Validation:

Table-1.: Comparison of present numerical results with published results of Khan et al. [26] for $M = K = \delta_1 = \delta_2 = Le = 0$

Pr	Present Nusselt number results	Nusselt number results of Khan et al. [26]
7.0	2.4365644434	2.404797
13.0	2.6697649859	2.705551
25.0	3.2799887563	3.287794
50.0	4.1377665750	4.115197
100.0	5.3454437548	5.336685

Table 1 shows a comparison between the latest Nusselt number (rate of heat transfer) findings and those published earlier by Khan et al. [26] utilising the shooting technique with the fourth- to fifth-order Runge-Kutta integration method. The second one failed to take the following factors into consideration: Lewis number, velocity slip, thermal slip, porous media, and magnetic field. You can see from the table that the new results are quite comparable to the ones published by Khan et al. [26].

5. Results and Discussion:

Various physical parameters, such as the Casson fluid parameter (β), magnetic field parameter (M), permeability parameter (K), velocity power index parameter (n), velocity slip parameter (δ_1), Prandtl number (Pr), thermophoresis parameter (Nt), Brownian motion parameter (Nb), thermal slip parameter (δ_2), and Lewis number (Le), are examined in this results and discussion section. The results are displayed in Figures 2–15 for dimensionless primary and secondary velocity profiles, temperature profit Additionally, using numerical values in tabular representations (Tables 2, 3, 4, and 5), the impacts of the same parameters on engineering quantities, such as skin-friction coefficients, Nusselt number (rate of heat transfer coefficient), and Sherwood number (rate of mass transfer coefficient), are explored. The following parameters have been set as fixed values for this research: $\gamma = 0.2$, $M = 0.3$, $K = 0.2$, $n = 0.1$, $\delta_1 = 0.5$, $Pr = 0.71$, $Nt = 0.1$, $Nb = 0.2$, $\delta_2 = 0.5$, and $Le = 0.4$.

5. 1. Effect of Casson fluid parameter (β): Through the use of the graphs shown in Figures 2 and 3, one is able to analyze the impact of Casson fluid parameter (varies from 0.2, 0.5, 0.8, 1.0), that various physical characteristics have on the primary and secondary velocity profiles. When the Casson fluid parameter is increased, the yield stress in the Casson nanofluid decreases. This phenomenon leads to a rise in the plastic dynamic viscosity, which in turn leads to an increase in the resistance to fluid flow. It is obvious that an increase in the flow barrier would cause the fluid's speed to decrease. As the Casson fluid parameter is increased, the graphical findings which are shown in Figures 2 and 3 demonstrate quite clearly that the velocity of the fluid decreases. As the Casson fluid parameter, the skin-friction coefficients are decreasing. This result is observed in tables 2 and 3.

5. 2. Effect of Magnetic field parameter (*M*): For different values of the magnetic field constant (0.3, 0.5, 0.7, and 1.0), Figs. 4 and 5 show the main and secondary velocity patterns. As the magnetic field parameter values rise, it can be seen that both of the velocity fields fall. A magnetic field tends to slow down the flow of liquids, which causes the thickness of the boundary layer for velocity and momentum to drop. Tables 2 and 3 show how variation in the magnetic field affects the skin-friction coefficients caused by the main and secondary velocity patterns. It can be seen from this table that as the magnetic field parameter value goes up, the skin-friction coefficients go down.

5. 3. Effect of Permeability parameter (*K*): This is seen in Figures 6 and 7, which show how the Permeability parameter (changes from 0.2, 0.5, 0.8, 1.0) influences the primary velocity profiles and the secondary velocity profiles, respectively. As a result of the inverse connection that exists between velocity profiles and the permeability parameter, numerical data demonstrates that the decrease in velocity profiles that occurs as the permeability parameter increases is a consequence of this relationship. As the permeability parameter increases, this process occurs as a result of the contemporaneous expansion of the porous layer, which results in a reduction in the thickness of the momentum barrier layer. In the tables 2 and 3, it is observed that, the skin-friction coefficients are decreasing with rising values of Permeability parameter.

5. 4. Effect of Velocity power index parameter (*n*): The effects of a velocity power index parameter of 0.1 on the skin-friction coefficient, 0.5 on the rate of heat transfer, and 0.9 on the mass transfer coefficient are detailed in Tables 2, 3, and 4, respectively. These statistics show that when the velocity power index parameter values grow, the skin-friction coefficients, rate of heat transfer, and mass transfer coefficients also increase.

5. 5. Effect of Velocity slip parameter (δ_1): Figure 8 shows how various values of the velocity slip parameter (0.5, 1.0, 1.5, and 2.0) change the velocity patterns. Increasing the velocity slip measure makes the fluid and stretched sheet move slower compared to each other. According to the experiment, as the velocity slip measure goes up, the nanofluid's speed goes down. According to tables 2 and 3, the velocity slip measure has an impact on the skin-friction coefficients because of the main and secondary velocity patterns. According to these data, as the velocity slip measure goes up, the skin-friction coefficients go down.

5. 6. Effect of Prandtl number (Pr): Figure 9 shows the connection between the Prandtl number (which can be 0.71, 1.0, 3.0, or 7.0) and the temperature of the stream being tested. As the Prandtl number keeps going up, the temperature difference in the fluid will appear less noticeable. It is the momentum diffusivity that finally becomes stronger than the heat diffusivity as the Prandtl number goes up. Momentum diffusivity finally passes temperature diffusivity, and this is what happens. Fluids probably can transfer heat faster or slower depending on how fast they are moving. The thickness of the border layer is immediately lowered, which makes heat move faster. The Prandtl number, or just "Prandtl number," affects the skin-friction coefficients and the rate of heat transfer coefficient. Tables 2, 3, and 4 show and talk about these effects. Based on the information in the charts, as the Prandtl number goes up, the skin-friction factors and the rate of heat movement tend to go down. The fact that this rate has been going down over time shows this.

Table-2.: Numerical values of $2\sqrt{\frac{n+1}{2}}.\left(1+\frac{1}{\beta}\right)Cf_x$ for different values of

β, M, K, n, δ_1, Pr, Nb, Nt, δ_2, and Le

β	M	K	n	δ_1	Pr	Nb	Nt	δ_2	Le	$2\sqrt{\frac{n+1}{2}}.\left(1+\frac{1}{\beta}\right)Cf_x$
0.2	0.3	0.2	0.1	0.5	0.71	0.2	0.1	0.5	0.4	3.165767556956561
0.5										3.110765871263087
0.8										3.086797690163445
	0.5									3.107695087620672
	0.7									3.053454354645435
		0.5								3.126875645208756
		0.8								3.105636572302524
			0.5							3.197687253087126
			0.9							3.219602646592525
				1.0						3.134658280368027
				1.5						3.107697926948562
					1.00					3.116595146795235
					3.00					3.086572084658256
						0.4				3.186750316409769
						0.6				3.216658259746195
							0.3			3.207685620569265
							0.5			3.226577648235786
								1.0		3.144141427659609
								1.5		3.107876983769162
									0.8	3.120886875645252
									1.2	3.096670659862097

5. 7. Effect of Brownian motion parameter (*Nb*): According to the information in Figs. 10 and 11, when the Brownian motion parameter (which ranges from 0.2 to 0.8), which describes the motion of the particles, goes up, the temperature goes up and the concentration fields go down. There are differences between nanoparticles in their thermophoresis and Brownian motion factors. These five tables display the mass transfer coefficients, the rate of heat transmission, and the skin friction coefficients. These tables are subject to alter according to the Brownian motion constant. When the value of the Brownian motion parameter increases, the skin-friction and heat transfer coefficients both rise, which may cause a decrease in the rate of mass transfer. It has the unintended consequence of having the reverse impact on the rate of mass transfer metric.

Table-3.: Numerical values of $2\sqrt{\frac{n+1}{2}}.\left(1+\frac{1}{\beta}\right)Cf_y$ for different values of

β, M, K, n, δ_1, Pr, Nb, Nt, δ_2, and Le

β	M	K	n	δ_1	Pr	Nb	Nt	δ_2	Le	$2\sqrt{\frac{n+1}{2}}.\left(1+\frac{1}{\beta}\right)Cf_y$
0.2	0.3	0.2	0.1	0.5	0.71	0.2	0.1	0.5	0.4	2.676305617592601
0.5										2.634760562085362
0.8										2.606776502659695
	0.5									2.645560872685765
	0.7									2.614657645287568
		0.5								2.635465243593563
		0.8								2.608769876973190
			0.5							2.724862358762538
			0.9							2.796797017265063
				1.0						2.625065716079265
				1.5						2.585487680573208
					1.00					2.626645283650785
					3.00					2.575676580658252
						0.4				2.705672506205876
						0.6				2.728658629385681
							0.3			2.736562058702295
							0.5			2.758406876218056
								1.0		2.648568256380972
								1.5		2.614395249585982
									0.8	2.635480250786341
									1.2	2.607696780762571

Table-4.: Numerical values of Nu_x for different values of n, Pr, Nb, Nt, and δ_2

n	Pr	Nb	Nt	δ_2	Nu_x
0.1	0.71	0.2	0.1	0.5	1.568756018650167
0.5					1.525085087532082
0.9					1.496106569602560
	1.00				1.516576571026078
	3.00				1.486787930146141
		0.4			1.596763760134961
		0.6			1.624547965380476
			0.3		1.616459285682952
			0.5		1.635480857628051
				1.0	1.516560915690760
				1.5	1.486670166785768

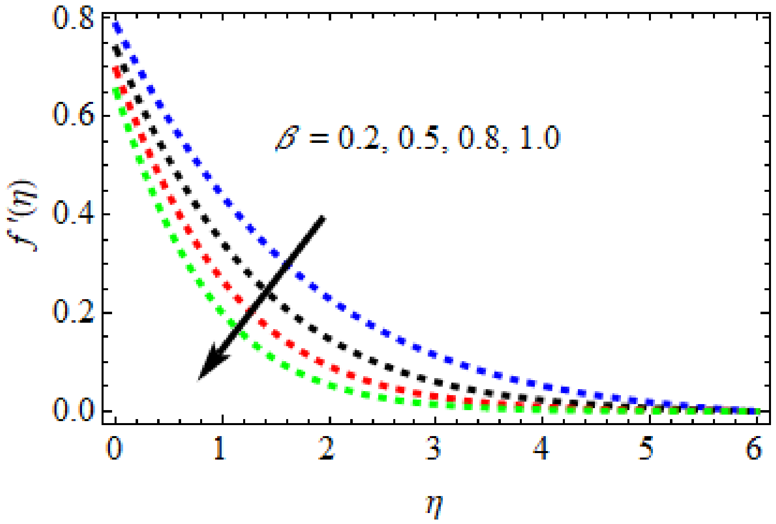

Fig. 2. Graph of primary velocity profiles for different values of β.

<u>5. 8. Effect of Thermophoresis parameter (*Nt*):</u> When you change the Thermophoresis parameter values to 0.1, 0.3, 0.5, or 0.7, you can see that both the temperature and concentration trends go up (Figs. 12 and 13). The thermophoresis measure is used a lot to figure out how thick the border layers are between temperature and concentration ranges. Because of this, both personalities have gotten better. In Tables 2, 3, 4, and 5, we look at how the thermophoresis parameter changes skin friction, heat transfer rates, and mass transfer factors. The factors of skin friction, heat transfer rate, and mass transfer all go up as the number of the thermophoresis measure goes up.

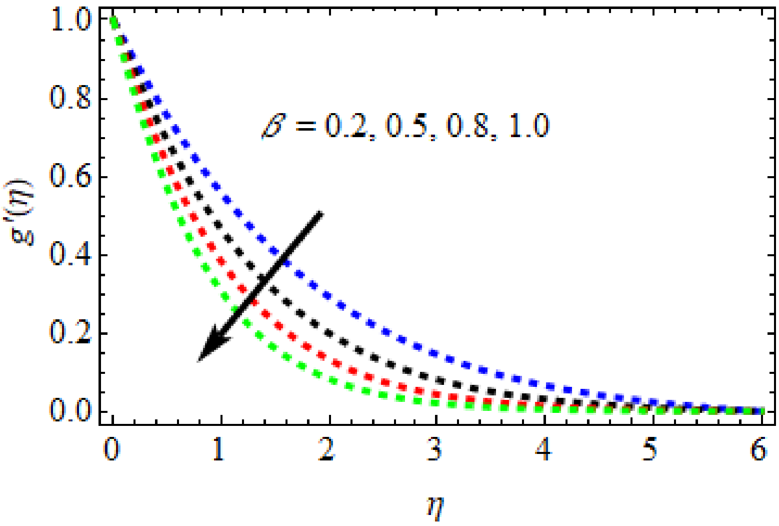

Fig. 3. Graph of secondary velocity profiles for different values of β.

5. 9. Effect of Thermal slip parameter (δ_2): Figure 14 displays how temperature curves change when the thermal slip measure changes from 0.5 to 1.0, 1.5 to 2.0. Depending on the flow conditions and the features of the material, the thermal slip measure can change the temperature patterns. When the thermal slip number is raised, heat doesn't move as easily from the solid surface to the fluid, so the temperature profile usually goes down. The fluid can "slip" away from the surface because of thermal slip, which lowers the contact area and, by extension, the rate of heat transfer. Figures 2, 3, and 4 show that as the Thermal slip parameter goes up, the skin-friction coefficients and the rate of heat transfer coefficient go down.

Table-5.: Numerical values of Sh_x for different values of *n*, *Nb*, *Nt*, and *Le*

n	Nb	Nt	Le	Sh_x
0.1	0.2	0.1	0.4	2.325420572856065
0.5				2.286765019625625
0.9				2.253325433545253
	0.4			2.296465087162581
	0.6			2.264576954325858
		0.3		2.354695253689569
		0.5		2.386756120876587
			0.8	2.275462549621229
			1.2	2.245674527982356

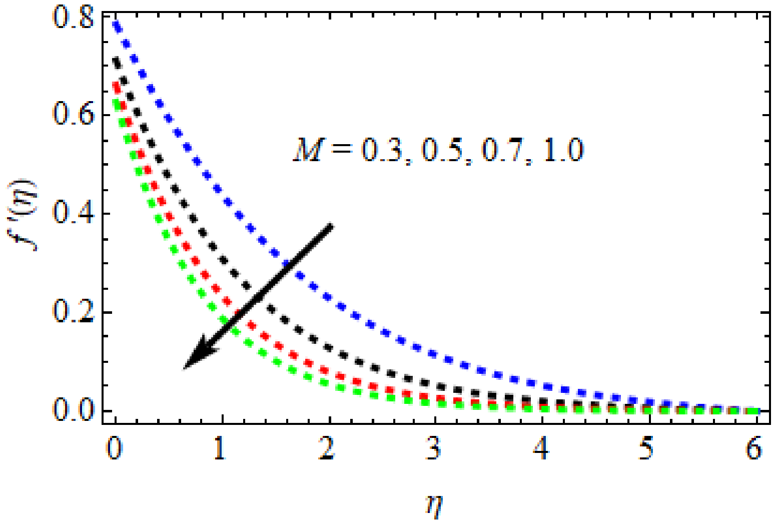

Fig. 4. Graph of primary velocity profiles for different values of *M*.

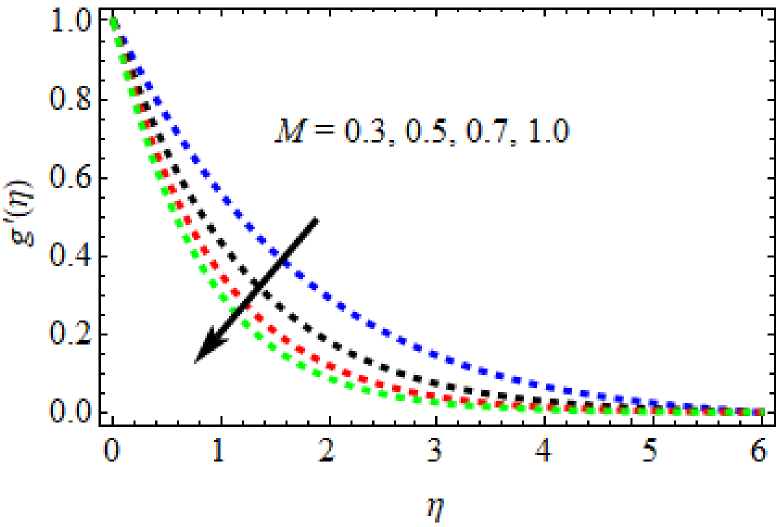

Fig. 5. Graph of secondary velocity profiles for different values of *M*.

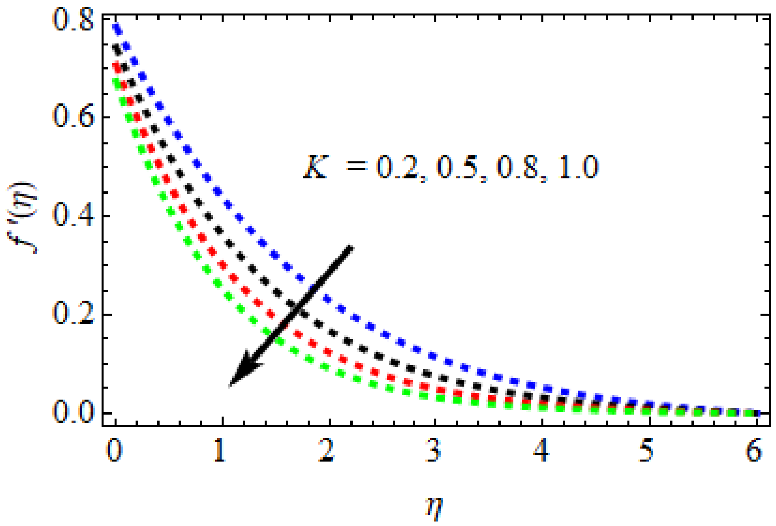

Fig. 6. Graph of primary velocity profiles for different values of *K*.

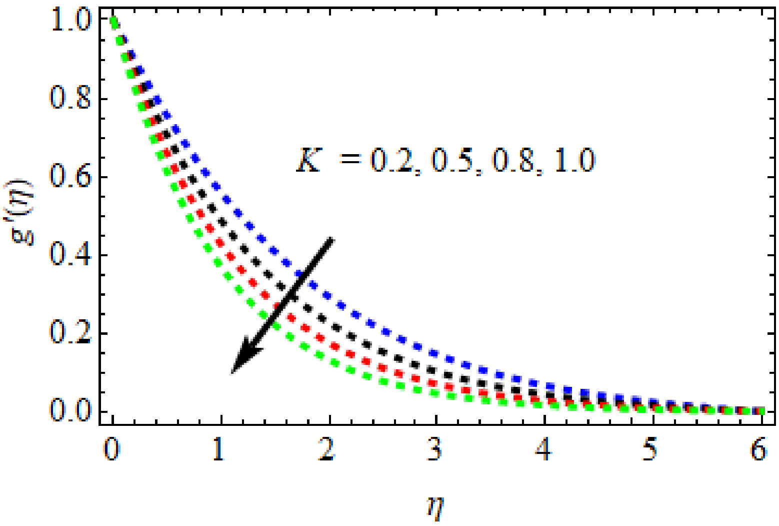

Fig. 7. Graph of secondary velocity profiles for different values of *K*.

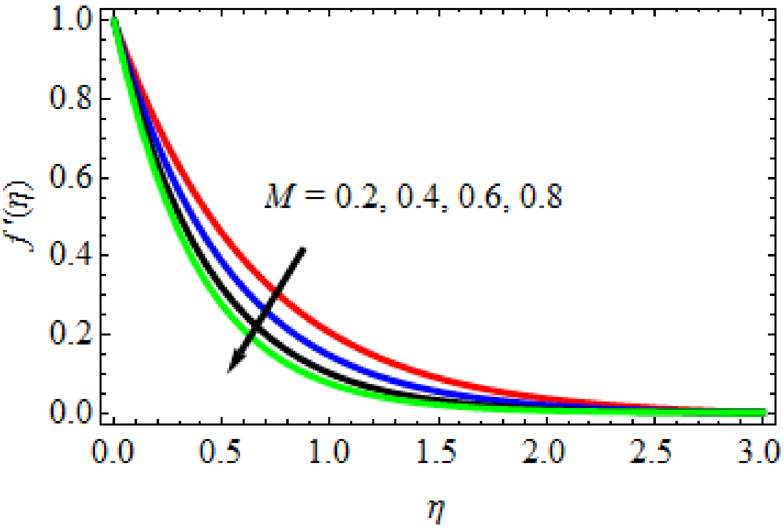

Fig. 8. Graph of primary velocity profiles for different values of δ_2.

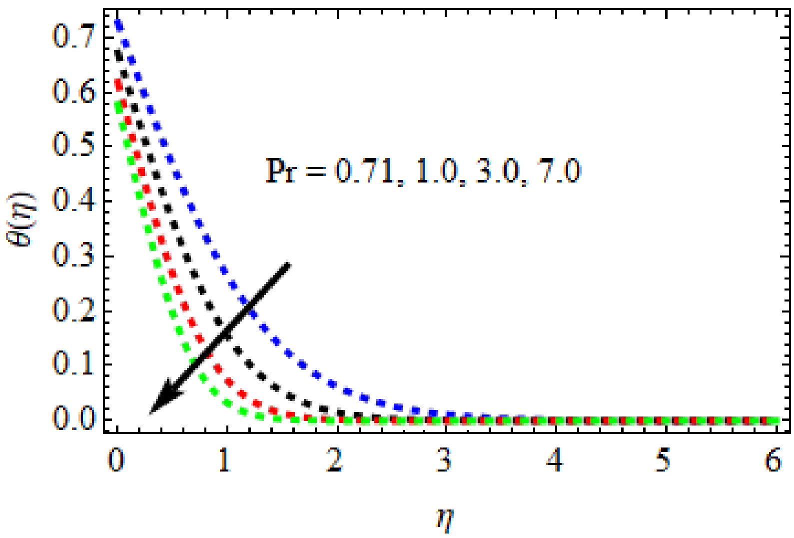

Fig. 9. Graph of temperature profiles for different values of Pr.

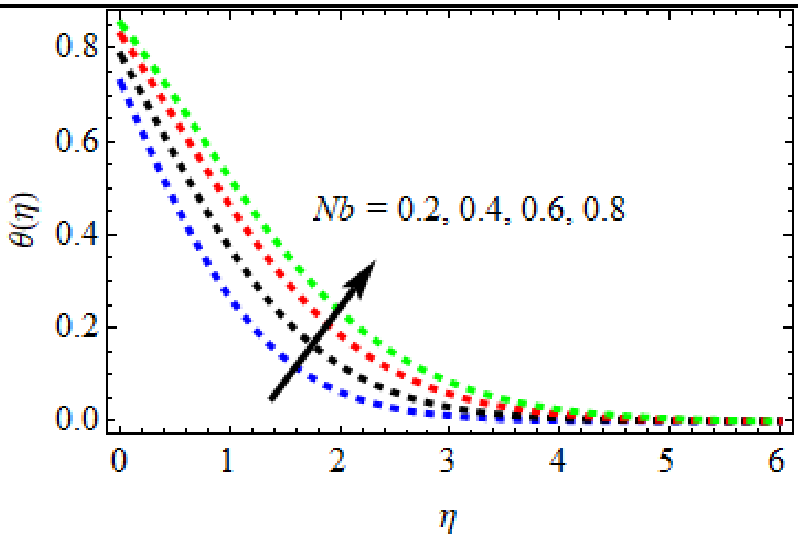

Fig. 10. Graph of temperature profiles for different values of *Nb*.

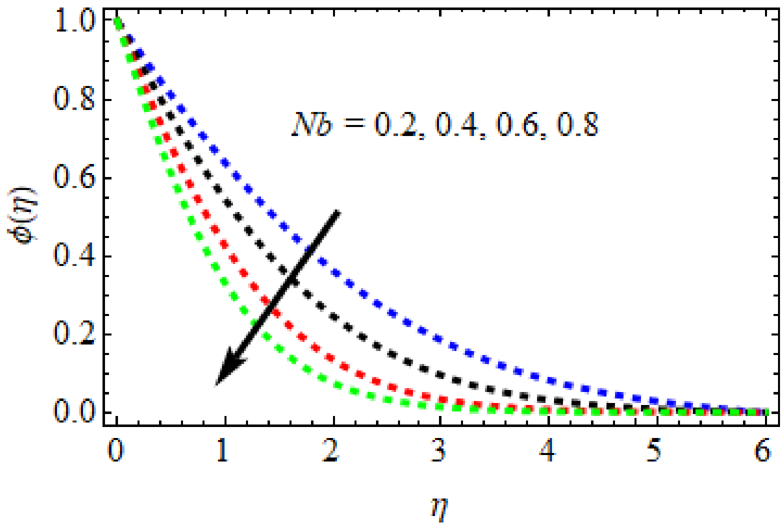

Fig. 11. Graph of Concentration profiles for different values of *Nb*.

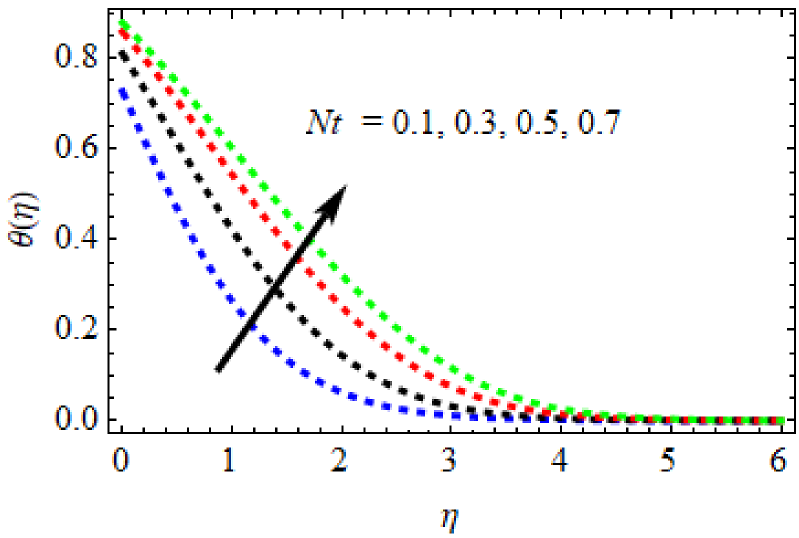

Fig. 12. Graph of temperature profiles for different values of *Nt*.

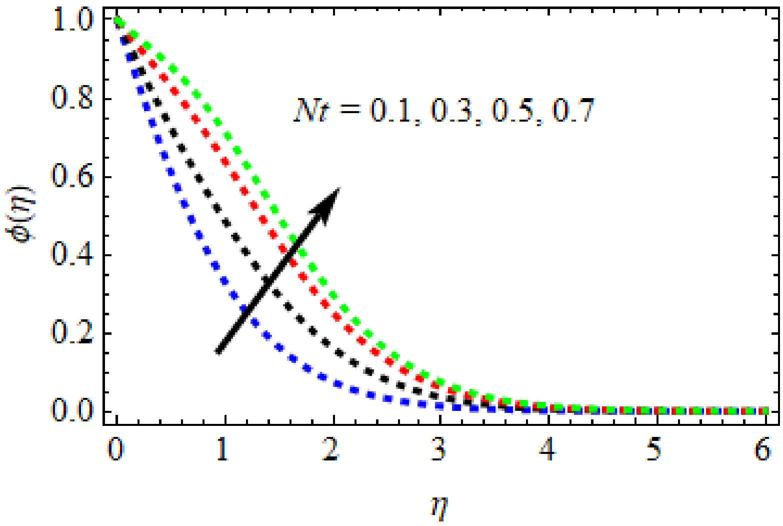

Fig. 13. Graph of concentration profiles for different values of Nt.

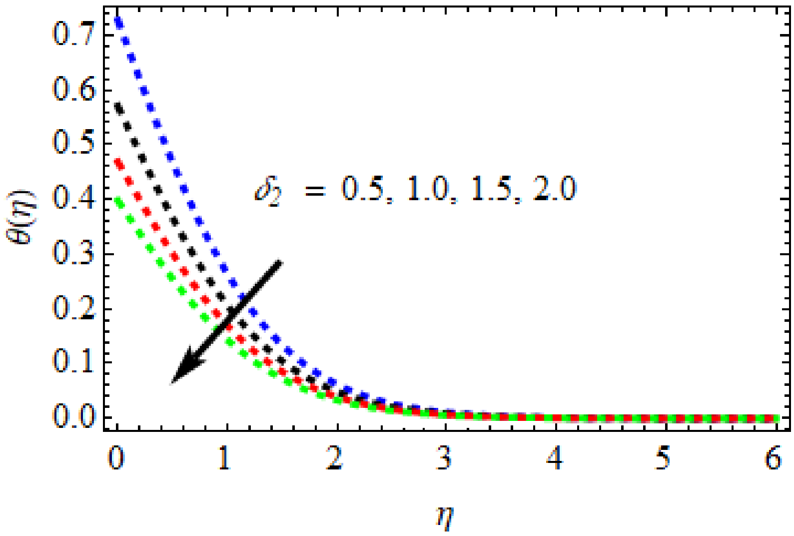

Fig. 14. Graph of temperature profiles for different values of δ_2.

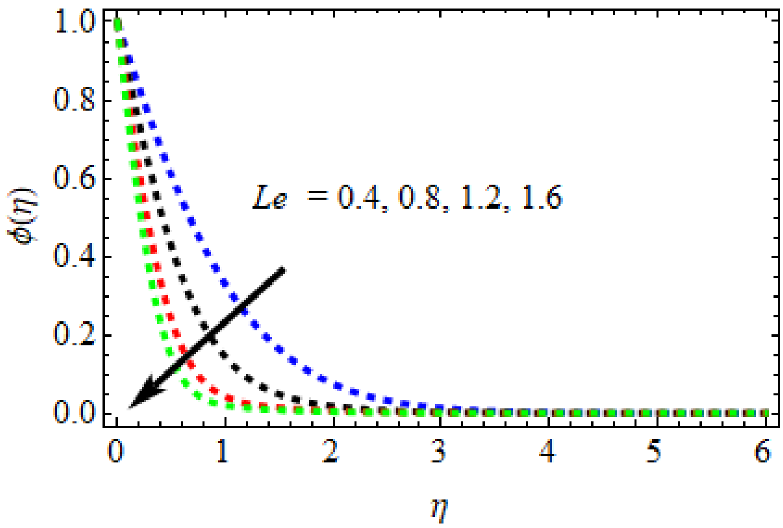

Fig. 15. Graph of concentration profiles for different values of *Le*.

6. **10. Effect of Lewis number (*Le*):** Figure 15 shows how the Lewis number (values from 0.4, 0.8, 1.2, 1.6) affects dimensionless concentration patterns. The proportion of heat and mass diffusivities is known as the dimensionless Lewis number. Lewis number causes the thermal boundary layer to thicken while the volume concentration of nanoparticles causes the nanoparticle boundary layer to thin. Tables 2, 3, and 5 correspondingly examine how the Lewis number influences the rate of mass transfer and the coefficients of surface friction. These results imply that surface friction and mass transfer rate factors decrease as the Lewis number increases.

7. Conclusions:

We looked at how a steady flow of Casson nanofluid across a flexible sheet can be modelled numerically in a porous medium with magnetic field and multiple slip effects. We also prove the results' correctness by comparing them to earlier results that were based on a few narrow assumptions. They match up pretty well. We studied how important thermophysical factors affected the dimensionless flow fields and here's what we found:

a) As the magnetic field constant goes up, the fluid speeds slowdown in both the x and y directions because of the Lorentz force.

b) The main and secondary velocity curves get smaller as the Permeability and Casson fluid factors get bigger.

c) The main velocity curves get smaller as the velocity slip parameter goes up.

d) As the Prandtl number goes up, temperature profiles go down, and as the Thermophoresis parameter and Brownian motion parameter go up, the opposite happens.

e) The concentration curves get smaller as the Thermophoresis parameter goes up, and the same is true for the Brownian motion parameter and the Lewis number.

f) To make sure the program code is correct, the writers compared this study to the data released by Khan et al. [26] and found that they agreed with each other.

References:

1. F. Mabood, S. Stanford, Multiple slip effects on MHD unsteady flow heat and mass transfer impinging on a permeable stretching sheet with radiation, Modeling and Simulation in Engineering 2019 (2019).
2. S. Eleni, E. Haile, T. Walelign, Multiple slips, Soret and Dufour effects in fluid flow near a vertical stretching sheet in the presence of magnetic nanoparticles, Int. J. Thermofluid., 13 (2022), Article 100136.
3. K. Shahid Ali, Yufeng Nie, Bagh Ali, Multiple slip effects on magnetohydrodynamic axisymmetric buoyant nanofluid flow above a stretching sheet with radiation and chemical reaction, Symmetry, 11 (9) (2019), p. 1171, 10.3390/sym11091171.
4. S. A. Khan, Y. Nie, B. Ali, Multiple slip effects on MHD unsteady viscoelastic nanofluid flow over a permeable stretching sheet with radiation using the finite element method, SN Appl. Sci., 2 (2020), p. 66, 10.1007/s42452-019-1831-3.

5. F. Soltani, L. Yilmazer, Slip velocity and slip layer thickness in flow of concentrated suspensions, J. Appl. Polym. Sci., 70 (2010), pp. 515-522.
6. Kuppala R. Sekhar, G. Viswanatha Reddy, C. S. K. Raju, S. M. Ibrahim, and O. D. Makinde, Multiple slip effects on magnetohydrodynamic boundary layer flow over a stretching sheet embedded in a porous medium with radiation and joule heating, Spec. Top Rev. Porous Media Int. J., Vol. 9, No. 2, pp. 117–132.
7. E. O. Atunmbi, A. Adeniyan, Heat and Mass Transfer in MHD micropolar fluid flow over a stretching sheet with velocity and Thermal slip conditions, Open J. Fluid Dynam., 8 (2018), pp. 195-215, 10.4236/ojfd.2018.82014.
8. C. S. K. Raju, P. Priyadarshini, S. M. Ibrahim, Multiple slip and cross diffusion on MHD Carreau-Casson fluid over a slandering sheet with non-uniform heat source/sink, Int. J. Algorithm. Comput. Math., 3 (2017), pp. 203-224.
9. S. Hussain, A. Aziz, T. Aziz, C. M. Khalique, Slip flow and heat transfer of nanofluids over a porous plate embedded in a porous medium with temperature dependent viscosity and thermal conductivity, Appl. Sci., 6 (12) (2016), p. 376.
10. K. Ganesh Kumar, G. K. Ramesh, B. J. Gireesha, A. M. Rashad, On stretched magnetic flow of Carreau nanofluid with slip effects and nonlinear thermal radiation, Nonlinear Eng., 8 (1) (2019), pp. 340-349.
11. A. Alsenafi, M. Ferdows, Effects of thermal slip and chemical reaction on free convective nanofluid from a horizontal plate embedded in a porous media, Math. Biosci. Eng., 18 (4) (2021), pp. 4817-8.
12. T. Sajid, W. Jamshed, F. Shahzad, M. A. Aiyashi, M. R. Eid, K. S. Nisar, A. Shukla, Impact of Maxwell velocity slip and Smoluchowski temperature slip on CNTs with modified Fourier theory: Reiner-Philippoff model, PLoS One, 16 (10) (2021), Article e0258367833.
13. A. Aziz, W. Jamshed, Unsteady MHD slip flow of Non-Newtonian power-law nanofluid over a moving surface with temperature dependent thermal conductivity, Discrete Continuous Dyn. Syst. - Ser. S, 11 (4) (2018).
14. M. Awais, T. Hayat, A. Ali, S. Irum, Velocity, thermal and concentration slip effects on a magneto-hydrodynamic nanofluid flow, Alex. Eng. J., 55 (3) (2016), pp. 2107-21